7-31-2018

All Diamond Microfiber Electrodes for Neuroelectrochemistry

Cory A. Rusinek
University of Nevada, Las Vegas, cory.rusinek@unlv.edu

Yue Gue
Michigan State University

Robert Rechenberg
Michigan State University

Michael F. Becker
Michigan State University

Erin Purcell
Michigan State University

See next page for additional authors

Journal of The Electrochemical Society

The Electrochemical Society
Advancing solid state & electrochemical science & technology

OPEN ACCESS

All-Diamond Microfiber Electrodes for Neurochemical Analysis

To cite this article: Cory A. Rusinek *et al* 2018 *J. Electrochem. Soc.* **165** G3087

JES Focus Issue on the Brain and Electrochemistry Honoring R. Mark Wightman and Christian Amatore

All-Diamond Microfiber Electrodes for Neurochemical Analysis

Cory A. Rusinek,[1,=,z] Yue Guo,[2,=] Robert Rechenberg,[1] Michael F. Becker,[1] Erin Purcell,[2,3] Matthew Verber,[4] Collin McKinney,[4] and Wen Li[2,3,z]

[1]*Fraunhofer USA, Inc. Center for Coatings and Diamond Technologies, Michigan State University, East Lansing, Michigan 48824, USA*
[2]*Department of Electrical and Computer Engineering, Michigan State University, East Lansing, Michigan 48824, USA*
[3]*Department of Biomedical Engineering, Michigan State University, East Lansing, Michigan 48824, USA*
[4]*Department of Chemistry, University of North Carolina at Chapel Hill, Chapel Hill, North Carolina 27599-3290, USA*

Neurochemical sensing with implantable microelectrodes has created multiple research opportunities in the field of neuroscience. The ability to record extracellular biopotentials and detect neurotransmitters with high sensitivity has enabled deeper understanding of brain and nervous system function. Diamond has many advantages over other electrode materials such as good biocompatibility, wide potential window, low double-layer capacitance, long-term stability, resistance to corrosion/fouling, and fabrication flexibility. In this work, we present a micromachined, implantable, all-diamond microfiber capable of reliable, precise neurochemical sensing. The all-diamond fiber consists of a conductive boron-doped polycrystalline diamond (BDD) core encapsulated in layers of insulating polycrystalline diamond (PCD) cladding. The PCD serves as a biocompatible and hermetic package while also acting as a dielectric barrier to prevent signal cross-talking. The all-diamond microelectrodes were thoroughly characterized using topographical and electrochemical methods. The capability for neurotransmitter sensing was completed using dopamine (DA) as the model analyte. Fast-scan cyclic voltammetry (FSCV) of DA was also completed to demonstrate the practicality for in vivo sensing at rapid rates. The fabrication is described in great detail and the capability for batch-scale process is demonstrated. These novel all-diamond microelectrodes have commercial-scale potential, generating a powerful tool for neurochemical analysis.
 [DOI: 10.1149/2.0141812jes]

Manuscript submitted April 30, 2018; revised manuscript received July 6, 2018. Published July 31, 2018. *This paper is part of the JES Focus Issue on the Brain and Electrochemistry Honoring R. Mark Wightman and Christian Amatore.*

The regulatory mechanisms and role of neurotransmitters (NTs) in brain function have long been of interest to chemists, neuroscientists, and physicians alike.[1–9] More specifically, NTs such as dopamine, serotonin, epinephrine, and nor-epinephrine belong to the catecholamine family and control many crucial physiological processes in both the brain and the peripheral nervous system (PNS).[8,10–13] Additionally, abnormalities in NT regulation or concentration can lead to several neurodegenerative disorders such as Parkinson's disease, Alzheimer's disease, depression, seizure, and schizophrenia.[5,6,8,14–18] As such, the capability to measure NTs generates a deeper understanding of brain function. Chemical sensing in the brain, however, is challenging due to a number of issues: low analyte concentration, presence of numerous interferences, risk of tissue damage, among many others. This environment can also cause significant sensor fouling and/or deactivation.[8,9]

Several different materials have been thoroughly investigated for neuroelectrochemical sensing and reports are bountiful.[8,9,19–25] The small electrode surface area and low capacitance allows for the measurement of small currents at fast scan rates ($\geq$100 V/s).[8,9,26–35] Carbon-fiber microelectrodes (CFMEs) are commonly found throughout literature and have proven capable of detection of a number of NTs. The Wightman Group pioneered much of the work on the use of CFMEs and in conjunction with Ralph Adams' prior work, paved the way for electrochemical measurements in the brain. CFMEs are typically housed in fused-silica capillaries.[8,9] For these glass-based electrodes, typical procedures include aspirating a single carbon fiber into a borosilicate glass capillary (dimensions: outer diameter 0.6–1.0 mm, inner diameter 0.4–0.5 mm).[8,9] After aspiration, the capillary is pulled on a commercial glass-electrode puller, leaving a tapered seal around the single carbon fiber.[8,9] CFMEs, however, are fragile (due to the fact that the thin layer of insulating borosilicate glass is more resistant to bending than the carbon fiber itself), difficult to manufacture, and can vary from electrode to electrode.[8,9] Furthermore, it is important to consider that scale-up and batch fabrication processes of CFMEs are difficult.[8] Other microsensors include metal-based or silicon-based (Si) electrodes and these have proven to be effective for neural stimulation and electrophysiology studies.[20,36–39] Such microsensors like the 'Michigan style' probe and 'Utah Array' offer the advantage of many different electrodes to record electrophysiology in larger tissue areas/samples.[20,36–38] Nevertheless, metal-based electrodes are susceptible to fouling through corrosion, passivation, and surface oxidation.[8,9] As such, a commercial microsensor which can be batch fabricated to generate reproducible and reliable results is still of significant interest and need.

Boron-doped diamond (BDD) is an excellent electrochemical tool. It offers advantages over metal-based and other carbon-based materials due to its large potential window, low background current, and excellent biocompatibility.[40–45] BDD can be fabricated in many different geometries and morphologies; microfabrication techniques can be readily found throughout literature.[40–45] BDD has also been investigated for its ability to measure NTs both in vivo and ex vivo.[40,46–50] This has included BDD micro- and nanoelectrode arrays (MEAs and NEAs), BDD-coated tungsten (W) and platinum (Pt) wires, and some larger-scale studies using BDD films on Si substrates where parameters such as film thickness and crystal size have been investigated.[49,51] Many of these studies, while interesting and relevant, fall short of a diamond-based device which could be made commercially available for continuous NT measurements in the brain and/or the PNS. In addition, these existing devices incorporate other metal or semiconductor materials that are vulnerable to biological environment, thereby increasing the risk of device corrosion/failures under chronic implantation. We recently reported on the fabrication and characterization of flexible BDD sensors for NT sensing.[40] The BDD film was grown on a Si substrate before a wafer transfer process was executed to place the BDD film on a flexible, biocompatible Parylene C substrate.[40]

In this paper, we report an all-diamond microfiber (μ-fiber) sensor capable of recording extracellular NT concentrations in neural networks. The sensor contains a μ-fiber shank and a contact pad on the backbone of the shank, as shown in Fig. 1A. Each shank consists of a BDD core encapsulated in a thin insulating, non-conducting polycrystalline diamond (PCD) cladding. The BDD core has a small

[=]These authors contributed equally to this work.
[z]E-mail: crusinek@fraunhofer.org; wenli@msu.edu

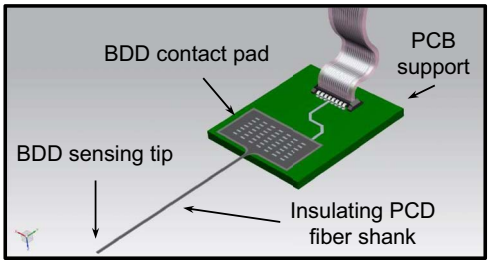

Figure 1. Conceptual diagram of the diamond μ-fiber.

cross-sectional area that matches the size of neurons, allowing for single-unit recording and NT measurements with high spatiotemporal resolution. The PCD cladding serves as a biocompatible, pinhole-free layer as well as a dielectric barrier to prevent signal cross-talking. The contact pad, which is made out of BDD, can be bonded onto a custom-designed, printed circuit board (PCB) using conductive silver paste for proper electrical connection and mechanical stability.

These freestanding, all- diamond μ-fibers differ from the conventional diamond electrodes discussed above as there is no additional support structure/substrate. A wafer-level microfabrication approach is developed for batch production of microfibers with various geometries (single fibers and 2D fiber arrays) and dimensions. The fabrication of these diamond μ-fiber electrodes is described with a detailed electrochemical characterization as well. Dopamine (DA) was used as the target NT analyte; an initial feasibility study using fast scan cyclic voltammetry (FSCV) was completed.

Experimental

Chemicals and materials.—Phosphate buffered saline (PBS) was purchased from Gibco and diluted with deionized (DI) water from 10X (10.6 mM monobasic potassium phosphate, 1551 mM sodium chloride, 29.7 mM dibasic sodium phosphate) to 1X (1.1 mM monobasic potassium phosphate, 155 mM sodium chloride, 3.0 mM dibasic sodium phosphate) for a final pH of 7.4. Potassium ferrocyanide ($K_4Fe(CN)_6$ and potassium ferricyanide ($K_3Fe(CN)_6$ were purchased from J.T Baker; Hexaamine-ruthenium(III) chloride ($Ru(NH_3)_6Cl$, hydroquinone (HQ), and dopamine (DA) were purchased from Sigma Aldrich. 50 mM stock solutions were prepared by dissolving the analyte of interest in the 1X, pH 7.4 PBS buffer. For the 3-electrode experiments, a silver/silver chloride (Ag/AgCl) reference electrode (Bioanalytical Systems, Inc.) was used while a homemade 2 mm ∅, freestanding BDD disk electrode was used as the counter electrode (Fraunhofer USA, Inc. CCD). For the 2-electrode FSCV experiments, the Ag/AgCl reference electrode was used.

Instrumentation.—For the three-electrode experiments, CHI 660C (CH Instruments) and Autolab PGSTAT 128 N potentiostats where used. All experiments were conducted in a Faraday cage and a picoamp booster was used with the CHI 660C. A mini-UEI system and HDCV Acquisition and Analysis software were used to perform FSCV measurements.[52,53] This system and software were designed by the Electronics Design Facility in conjunction with Professor Mark Wightman in the Chemistry Department of the University of North Carolina at Chapel Hill.

BDD microfiber fabrication.—The BDD μ-fiber electrodes were fabricated using a multi-step microfabrication process where a triple layer of un-doped, boron-doped and un-doped microcrystalline diamond (MCD) is fabricated to yield individual diamond μ-fibers. Each μ-fiber contains an electrically conductive BDD core entirely enclosed in an electrically insulating PCD cladding, except for the sensing surface and contact pad. A schematic of the process flow is shown in Figs. 2A below.

In the first step, a dual layer of electrically insulating and electrically conductive diamond layers was grown on a 1 mm thick 3-inch-diameter (100) Si wafer. Each layer was grown in a dedicated in-house built 2.45 GHz microwave plasma assisted chemical vapor deposition (MPACVD) reactor. Both diamond growth processes had similar growth parameters of 25 Torr pressure, 1.6 kW absorbed microwave power resulting in a deposition temperature of 700°C. Gas flows were set to 1% methane (CH_4) in hydrogen (H_2) balance for high quality MCD growth. Diborane (B_2H_6) was added to the conductive diamond (BDD) growth process in a B/C ratio of 20,000 ppm to achieve sufficient conductivity. The resulting electrically insulating PCD diamond layer was 1.9 μm thick. The electrically conducting BDD layer was 3.7 μm thick and had a resistivity of 1×10^{-3} Ω∗cm.

During the second step the dual layer was etched to what will later on become the individual μ-fibers including fiber shank, contact pad and anchor. Prior to etching, a 1.2 μm thick copper (Cu) hard mask was thermally evaporated. (Edward Auto306 thermal evaporator, Edwards, Inc.). In order to enhance the adhesion between Cu and BDD, a 50 nm thick titanium (Ti) interlayer was thermally evaporated using the same equipment. Diluted Cu etchant (ferric chloride ($FeCl_3$) solution: DI water = 1:2 (vol/vol)) was used to smoothly pattern the Cu mask, and the Ti layer was later patterned by dry etching. A reactive ion plasma dry etcher (Lambda Technologies) was utilized to etch the masked diamond layers with a gas mixture of 0.8:6:20 sccm $SF_6/Ar/O_2$, 750 W microwave power and 160 V bias at 15 mTorr. Care was taken not to over etch the Si substrate since a smooth, properly etched Si surface is essential for the third processing step. After plasma etching, the remaining Cu mask was wet etched with the same diluted ferric chloride solution and the Ti layer was removed by buffered oxide etchant (Transene Company, Inc.).

In the third processing step, the final MCD cladding was performed enclosing the μ-fiber. A Ti/Cu mask was applied via a lift-off procedure to selectively mask the top of the contact pads, thereby inhibiting diamond growth during the final growth process. A 50 nm Ti/1.2 μm Cu layer was applied with the same system as listed above. For the final insulating diamond growth, the same MWPACVD reactor and process parameters were used as described above. A smooth and relatively undamaged Si surface is critical to allow diamond growth only on the exposed diamond on the wafer. The third and final MCD layer was 1.3 μm thick and electrically insulating as well.

In the fourth and final processing step, the μ-fibers were released from the Si substrate by back etching the Si substrate using a nitric acid/hydrofluoric acid/water (55:15:30) etching solution. Remarkably, the μ-fibers are strong enough to withstand this rather aggressive and turbulent etching, several rinsing steps and manual separation without breaking. Before mounting the μ-fibers onto a custom-made PCB board, the anchor is cleaved off from the μ-fiber shank exposing pristine BDD for subsequent analysis. This was done manually, using a sharp blade to carefully remove the anchor. This anchor structure was specifically designed to protect the μ-fiber tip from being contaminated by plasma etching. Scanning electron micrographs (SEM) of the resulting BDD μ-fibers are shown in Figs. 2B and 2C. In Figs. 2B, 3 individual fibers are shown still partially attached to the Si substrate. The Si substrate is completely removed prior to mounting. A top-view SEM image of a single fiber is inlayed in Fig. 2B, showing a 3 mm long fiber shank (measured from base to tip). An SEM of the conductive, BDD tip is shown in Fig. 2C. Both the BDD core and the PCD cladding consist of diamond crystal sizes on the order of 1–2 μm. The measured surface area of the BDD fiber core was ∼70 μm^2, exhibiting similar geometry to a band-type microelectrode. The overall cross-sectional area of the probe is 25 μm wide × 6 μm high. Because a given batch of μ-fiber electrodes would be exclusively fabricated from the same wafer (PCD/BDD deposition and patterning), each of them should be nearly identical. The BDD and PCD layers exhibit uniform crystallinity and conductivity (BDD only). This should allow for a reproducible BDD sensing area from fiber to fiber.

Prior to use in electrochemical measurements, the BDD μ-fibers were rinsed with acetone and methanol. Immediately after this cleaning step the μ-fibers were pre-conditioned and electrochemically

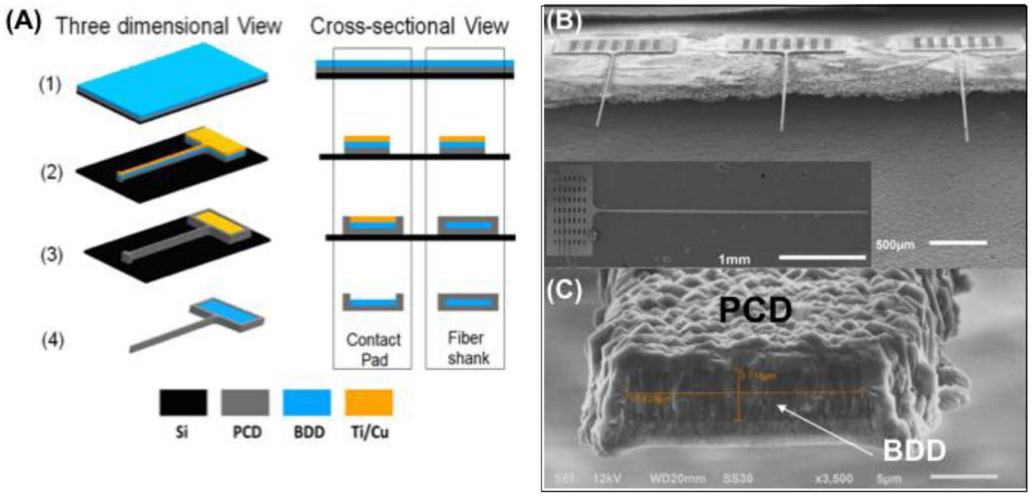

Figure 2. (A) Microfabrication process flow for making the all diamond μ-fibers. 1. Deposition of PCD and BDD thin film layers onto Si substrate; 2. Pattern Cu mask and plasma etching of PCD/BDD layers; 3. Pattern Cu mask and deposition of final PCD layer; 4. Cu removal, device release and fiber cleavage. (B) Scanning electron micrographs of the all-diamond μ-fiber electrodes. Inset shows a released single μ-fiber. (C) Cross-sectional image of the doped-diamond core surrounded by un-doped PCD cladding.

cleaned using cyclic voltammetry (CV) in 1.0 M H_2SO_4 by cycling the potential from 0.0 V to +2.8 V to −2.4 V before stopping back at 0.0 V. This potential range was swept 30 times at a scan rate of 0.5 V/s. We have found that this provides a clean, reproducible BDD surface before measurements are started.

Results and Discussion

Surface and material characterization.—With the deposition flexibility exhibited by BDD as a material, it is necessary to investigate the electrode surface on a case-by-case basis. Additionally, due to the complex nature of the fabrication process, characterization of both the un-doped PCD cladding and the doped PCD core (BDD) is needed. As such, the BDD μfibers were investigated using SEM (described above) and Raman spectroscopy.

Boron-doping effects the film surface morphology as well as the structure and electrochemical properties.[54–58] Raman spectroscopy is an excellent tool to evaluate diamond films and the spectra of the un-doped and doped layers are shown in Fig. 3. The Raman spectrum of the BDD shown in Figs. 3 suggests a highly-doped film, as indicated by the large, broad peaks at 500 and 1200 cm^{-1}, respectively.[59,60] Furthermore, based on the Lorentzian component of the boron peak at ∼500 cm^{-1}, the BDD film is considered to be heavily doped.[61] The diamond phonon is seen ca. 1300 cm^{-1}; this is the sharp peak shown in the PCD spectrum. This peak is attenuated in the BDD spectrum; however, this is slightly shifted due to the elevated boron content and subsequent doping level.

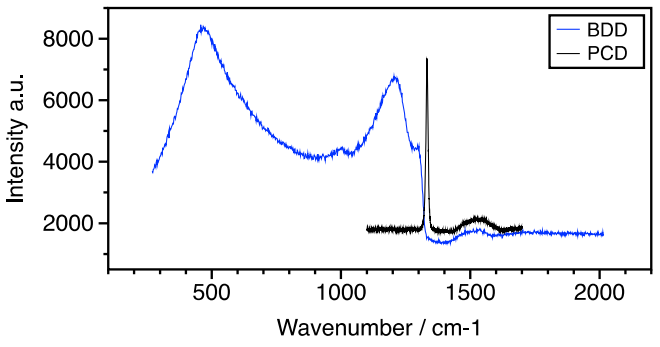

Figure 3. Raman spectra of the boron-doped polycrystalline diamond (BDD) and un-doped polycrystalline diamond (PCD) layers on the all-diamond μ-fiber sensor.

Electrochemical characterization.—Due to the novelty of the all-diamond μ-fiber electrodes, a thorough electrochemical characterization was completed using electrochemical impedance spectroscopy (EIS) and CV. The impedance at 1.0 kHz was found to be 1.3 MΩ (data not shown). This is comparable to CFMEs in literature. Background CV *i-E* curves were completed in 1.0 M H_2SO_4 and pH 7.4 PBS buffer to determine both the potential window and the double layer capacitance (C_{dl}); the curves are shown in Figs. 4A and 4B. The potential window was found to be ∼5.0 V in pH 7.4 PBS and ∼4.0 V in 1.0 M H_2SO_4. The wider window in PBS is due to the larger hydrogen overpotential stemming from the increased pH and subsequent lower number of H^+ available to be reduced to H_2 at the electrode surface. In both media, the BDD μ-fiber indicated featureless background current throughout the potential region of most redox active NTs. The peak ca. +2.25 V in the PBS CV is likely due to oxidation of the PBS itself as this peak is not apparent in the 1.0 M H_2SO_4 scan. The BDD μ-fiber potential window surpasses that of many other electrode materials, both carbon and metal-based. For the measurement of C_{dl}, the current (A) was measured at 0.0 V in the forward segment of the final CV scan (3 scans total) and plotted against scan rate (V/s); the slope was used to calculate C_{dl}.[45] Measurements were completed in triplicate. Using this methodology, C_{dl} was calculated to be ∼11 μF cm^{-2}, a typical value for diamond electrodes exhibiting low capacitance. Though the BDD μ-fibers are exposed to many different environments throughout the fabrication processes, it is important to note that the tip of the electrode is severed before analysis. This leaves behind a clean, non-contaminated BDD tip.

For further electrochemical characterization of the BDD μ-fibers, the behavior toward several traditional analytes was assessed. This included the ferri/ferrocyanide ($Fe(CN)_6^{3-/4-}$), hexamine ruthenium ($Ru(NH_3)_6^{2+/3+}$), and hydroquinone (HQ) redox couples and the CV *i-E* curves are shown in Fig. 4C. Excellent steady state response was achieved with each redox couple, indicating that the diffusion layer thickness is larger than the radius of electroactive BDD μ-fiber core ($(Dt^{1/2}) > r_0$).[62–65] Contrarily, when the diffusion layer is smaller than the electrode area ($(Dt^{1/2}) < r_0$), semi-infinite linear diffusion is observed and voltammetric peaks are seen.[62–65] As such, the smaller the electrode, the quicker steady-state conditions are achieved. This behavior is described at length by Kissinger, Heineman, Wightman, and Michael.[62]

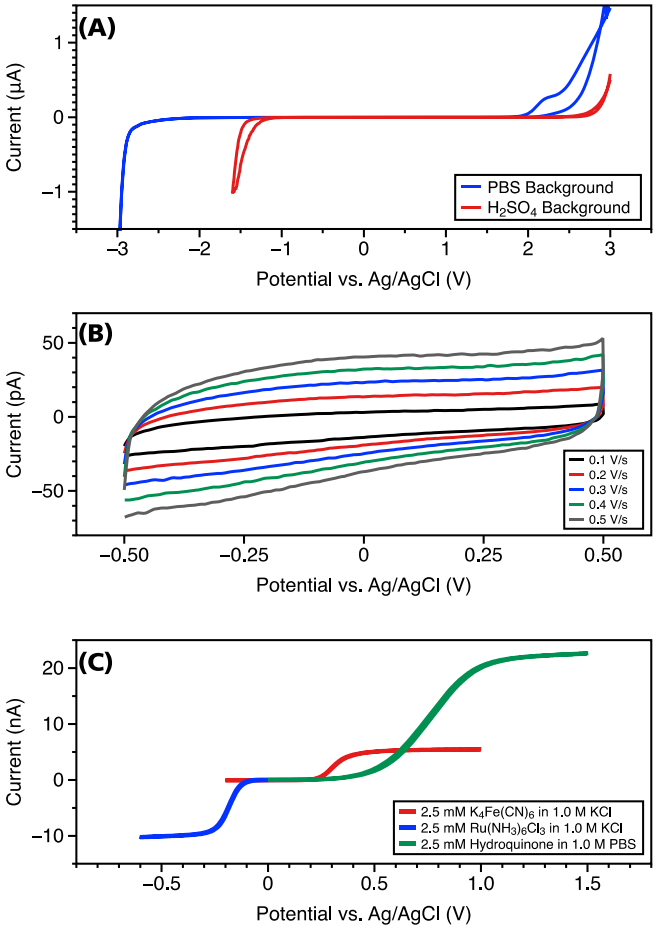

Figure 4. Cyclic voltammetric *i-E* curves obtained with the all-diamond μ-fiber electrodes. (A) potential window using 1.0 M H_2SO_4 and pH 7.4 PBS, (B) background voltammograms in pH 7.4 PBS for the calculation of C_{dl}, and (C) voltammograms of 2.5 mM $Fe(CN)_6^{3-/4-}$, 2.5 mM $Ru(NH_3)_6^{2+/3+}$, and 2.5 mM hydroquinone in pH 7.4 PBS. Reference electrode- Ag/AgCl, counter electrode- BDD disk. Scan rate for (C)- 0.1 V/s.

The electron transfer kinetics toward the $Fe(CN)_6^{3-/4-}$ couple (inner sphere electron transfer) is sensitive to the BDD surface morphology.[45] On the other hand, the $Ru(NH_3)_6^{2+/3+}$ redox couple is an outer sphere electron transfer reaction and thus, is not as sensitive to the BDD surface. However, as evident in Fig. 4C, excellent steady state current response was achieved for each redox couple. The HQ voltammogram exhibited larger current response but it is important to consider that this is a 2-electron transfer reaction, compared to the 1-electron transfer $Fe(CN)_6^{3-/4-}$ and $Ru(NH_3)_6^{2+/3+}$. Lastly, 5 BDD μ-fibers were individually tested for their response to the $Fe(CN)_6^{3-/4-}$ redox couple at concentrations of 1.0 and 2.5 mM at a scan rate of 0.1 V/s; the steady state current (i_{ss}) was measured at +0.8 V. The average sensitivity obtained at each fiber was 1.1 (± 0.3) nA/mM, indicating good precision from fiber to fiber. More detailed reproducibility studies are planned for future work.

Dopamine analysis.—Various BDD electrodes have been investigated for DA detection; this includes thin films on W and/or Pt wires as well as MEAs and NEAs.[46–48] Suzuki, Fujishima, and Einaga fabricated and characterized microelectrodes of BDD on W.[21] Additionally, they housed the BDD-coated W wire in a pre-pulled glass capillary tube, a similar fashion as to what is used for the construction of CFMEs. Using a series of electroanalytical measurements such as CV, chronoamperometry (CA), and differential pulse voltammetry (DPV), promising results were shown.[21] For FSCV, however, they did not investigate scan rates above 0.5 V/s. As stated previously, for practical DA sensing in the brain, microelectrodes must be capable of scanning at speeds much faster than this (>100 V/s). Others have investigated the "tunable" features of BDD for DA sensing such as film thickness, surface termination, and crystal size.[51] Due to the novelty of our BDD μ-fibers for this work, however, investigations of such parameters were considered out of scope.

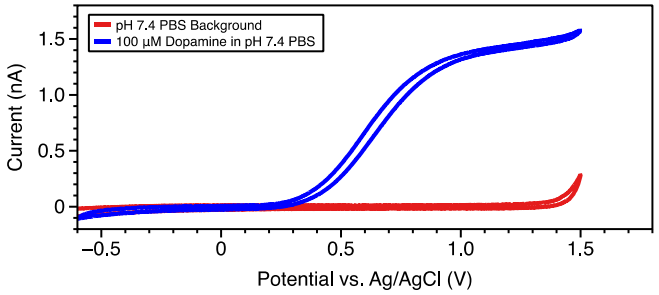

Figure 5. Dopamine CV *i*-E curve using the BDD μ-fiber in pH 7.4 PBS buffer. Scan rate- 1.0 V/s. [Dopamine]: 100 μM.

Prior to the feasibility investigation into FSCV, the BDD μ-fibers were characterized for the ability to detect DA by traditional CV measurements. Scan rates of 0.05 to 50 V/s were investigated; the data at a scan rate of 1.0 V/s is shown in Fig. 5. During the DA scan rate study, steady state current response was observed up to a scan rate of 5.0 V/s (data not shown). At higher scan rates, the transition from steady state conditions to voltammetric peaks is largely due to the change in the diffusion profile, discussed previously. Nonetheless, the response to DA occurs in the expected potential region and is similar to the of other reports in literature for BDD electrodes.[21,46,51]

Dopamine fast scan cyclic voltammetry.—To effectively measure DA transients in vivo, measurements must be executed on the milli-second (ms) time scale.[4,8,9] This is due to a combination of the neuron firing rate as well as diffusivity of DA into the extracellular space.[7–9,52,53] It is important to note that for any electroanalytical in vivo application, the microelectrode sits in the extracellular space around the target neuron.[7–9,52,53] In FSCV, the background charging current stabilizes after repeated cycling of the electrochemical potential and thus, can be subtracted from the measured faradaic current. This enables the sensing of rapid changes in analyte concentration (NT transients) at the ms scale.[4,8]

The color plot shown in Fig. 6A shows a time plot of a constant dopamine concentration and the inset shows a time plot of the background prior to addition of DA to the stagnant electrochemical cell. Future work will utilize a flow cell to calibrate the dopamine response of the BDD μ-fiber electrodes. Nonetheless, the color plot shows a solid current response from both the oxidation and reduction peaks for DA, signifying that the BDD μ-fibers exhibit the conductivity needed for FSCV. It should be noted from the data shown in Fig. 6B that the DA oxidation peak has shifted positively from Fig. 5. This is also slightly shifted positive from what is seen with CFMEs as well.[8,9] However, this is largely due to the increased resistivity of BDD as a material compared to the primarily sp^2-bonded carbon fiber.[42,45,46] While this positively shifted DA oxidation, peak may be an issue for a CFME, it is important to recall the electrochemical potential window data shown in Fig. 4A of the BDD μ-fiber. As such, a DA oxidation peak potential of ~ +1.05 V is still well within the analytical window for BDD. Additionally, the limited surface oxidation observed with BDD renders the concern over DA potential shift irrelevant.

Conclusions

In this paper, we report a novel, all-diamond μ-fiber electrode for neurochemical sensing. The electrode consists of a conductive BDD core with an insulating PCD cladding. During fabrication, the PCD/BDD/PCD layers were patterned and subsequently released from

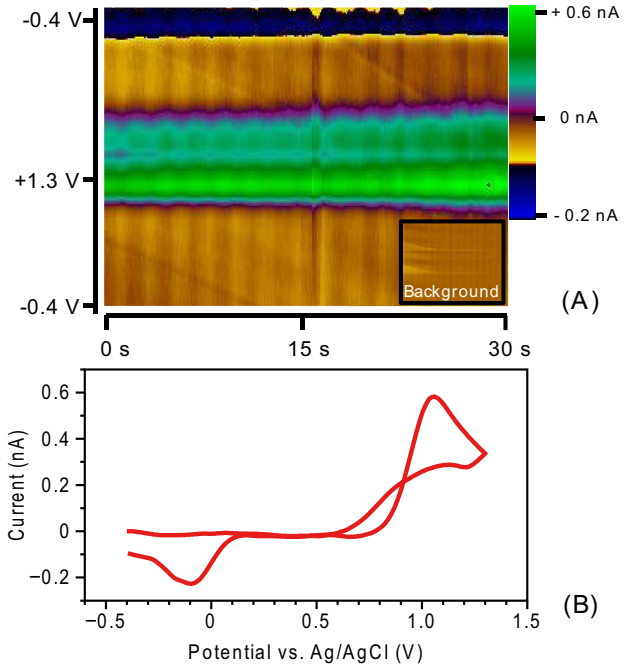

Figure 6. Dopamine FSCV in a stagnant electrochemical cell. (A) Color plot from HDCV software, courtesy of the University of North Carolina at Chapel Hill. (B) Individual FSCV *i*-E curve of DA in pH 7.4 PBS buffer. The FSCV color plot for the PBS buffer background is inlayed in (A). Scan rate- 400 V/s; Reference electrode- Ag/AgCl; [Dopamine]: 20 μM.

the Si substrate, leaving behind the freestanding μ-fibers. Raman and SEM were completed and a clear distinction between the BDD and PCD layers was observed. The calculated surface area of the conductive BDD core was ∼70 μm^2; the overall dimensions of the fiber were found to be 6 μm × 25 μm. Prior to analysis, the tip of each μ-fiber electrode was severed and pre-conditioned in 1.0 M H_2SO_4 by scanning a wide voltage range with CV (−2.4 V to +3.0 V). The diamond μ-fibers were then evaluated via an electrochemical characterization. In pH 7.4 PBS buffer, the potential window was ∼5.0 V and the C_{dl} was calculated to be 11 μF cm^{-2} (using the electrode surface area calculated with SEM). Three redox couples were also studied ($Fe(CN)_6^{3-/4-}$, $Ru(NH_3)_6^{2+/3+}$, and HQ); excellent steady-state conditions were achieved for each suggesting a hemispherical diffusion case, typical for microelectrodes of this size. The μ-fibers were also studied for their ability to detect DA in buffered samples. Several CV scan rates were used and it was found that the transition from steady-state conditions to a semi-infinite linear diffusive case ca. 5.0 V/s. Lastly, the μ-fibers were assessed for their capability to execute FSCV of DA. Using a concentration of 20 μM, a well-resolved voltammogram with quantifiable DA peaks was obtained at a scan rate of 400 V/s in a stagnant electrochemical cell. The peaks were slightly lower in magnitude compared to competing data obtained with CFMEs in literature; however, it is important to note that the surface area of the diamond μ-fibers is smaller than that of a cylindrical CFME. Future studies include an FSCV scan rate study, in-depth reproducibility across several analytes, incorporation of a flow-through system, and a thorough comparison with the performance of CFMEs. These novel μ-fiber electrodes can be batch fabricated to make hundreds, potentially thousands at once. With a repeatable electrode surface, a commercially available microelectrode for wide spread neuroelectrochemical applications can be achieved.

Acknowledgment

The authors gratefully acknowledge Madeline Mackinder for her help testing the BDD μ-fiber electrodes. The authors also acknowledge Dr. Bin Fan and Dr. Lindsay Walton for helpful discussions. The project was internally funded through a collaboration of the Michigan State University-Fraunhofer USA, Inc. Center for Coatings and Diamond Technologies.

ORCID

Cory A. Rusinek https://orcid.org/0000-0002-6852-0219

References

1. M. Hawley, S. Tatawawadi, S. Piekarski, and R. N. Adams, *Journal of the American Chemical Society*, **89**, 447 (1967).
2. R. N. Adams, *Electrochemistry at Solid Electrodes*, M. Dekker 1969.
3. P. T. Kissinger, J. B. Hart, and R. N. Adams, *Brain Research*, **55**, 209 (1973).
4. J. Millar, J. A. Stamford, Z. L. Kruk, and R. M. Wightman, *European Journal of Pharmacology*, **109**, 341 (1985).
5. S. W. Kuffler and J. G. Nicholls, *From Neuron to Brain*, Sinauer Associates, 1976.
6. E. R. Kandel, J. H. Schwartz, T. M. Jessell, S. A. Siegelbaum, and A. J. Hudspeth, *Principles of Neural Science*, McGraw-hill New York, 2000; Vol. 4.
7. D. Michael, E. R. Travis, and R. M. Wightman, *Analytical Chemistry*, **70**, 586A (1998).
8. J. G. Roberts and L. A. Sombers, *Analytical Chemistry*, **90**, 490 (2017).
9. N. T. Rodeberg, S. G. Sandberg, J. A. Johnson, P. E. Phillips, and R. M. Wightman, *ACS Chemical Neuroscience*, **8**, 221 (2017).
10. M. L. Heien, M. A. Johnson, and R. M. Wightman, *Analytical Chemistry*, **76**, 5697 (2004).
11. B. P. Jackson, S. M. Dietz, and R. M. Wightman, *Analytical Chemistry*, **67**, 1115 (1995).
12. K. Pihel, Q. D. Walker, and R. M. Wightman, *Analytical Chemistry*, **68**, 2084 (1996).
13. D. L. Robinson, B. J. Venton, M. L. Heien, and R. M. Wightman, *Clinical Chemistry*, **49**, 1763 (2003).
14. K. J. Barnham, C. L. Masters, and A. I. Bush, *Nature Reviews Drug Discovery*, **3**, 205 (2004).
15. W. Dauer and S. Przedborski, *Neuron*, **39**, 889 (2003).
16. M. A. Johnson, V. Rajan, C. E. Miller, and R. M. Wightman, *Journal of Neurochemistry*, **97**, 737 (2006).
17. C. Behl and B. Moosmann, *Biological Chemistry*, **383**, 521 (2002).
18. B. A. Yanker, *Nature Medicine*, **2**, 850 (1996).
19. J. J. Clark, S. G. Sandberg, M. J. Wanat, J. O. Gan, E. A. Horne, A. S. Hart, C. A. Akers, J. G. Parker, I. Willuhn, and V. Martinez, *Nature Methods*, **7**, 126 (2010).
20. S. Kim, R. Bhandari, M. Klein, S. Negi, L. Rieth, P. Tathireddy, M. Toepper, H. Oppermann, and F. Solzbacher, *Biomedical Microdevices*, **11**, 453 (2009).
21. A. Suzuki, T. A. Ivandini, K. Yoshimi, A. Fujishima, G. Oyama, T. Nakazato, N. Hattori, S. Kitazawa, and Y. Einaga, *Analytical Chemistry*, **79**, 8608 (2007).
22. M. K. Zachek, A. Hermans, R. M. Wightman, and G. S. McCarty, *Journal of Electroanalytical Chemistry*, **614**, 113 (2008).
23. W. Schultz, P. Apicella, and T. Ljungberg, *Journal of Neuroscience*, **13**, 900 (1993).
24. A. Fujishima, T. N. Rao, E. Popa, B. Sarada, I. Yagi, and D. Tryk, *Journal of Electroanalytical Chemistry*, **473**, 179 (1999).
25. A. E. Hess, D. M. Sabens, H. B. Martin, and C. A. Zorman, *Journal of Microelectromechanical Systems*, **20**, 867 (2011).
26. A. L. Sanford, S. W. Morton, K. L. Whitehouse, H. M. Oara, L. Z. Lugo-Morales, J. G. Roberts, and L. A. Sombers, *Analytical Chemistry*, **82**, 5205 (2010).
27. R. M. Wightman, M. L. Heien, K. M. Wassum, L. A. Sombers, B. J. Aragona, A. S. Khan, J. L. Ariansen, J. F. Cheer, P. E. Phillips, and R. M. Carelli, *European Journal of Neuroscience*, **26**, 2046 (2007).
28. P. R. Patel, K. Na, H. Zhang, T. D. Kozai, N. A. Kotov, E. Yoon, and C. A. Chestek, *Journal of Neural Engineering*, **12**, 046009 (2015).
29. P. R. Patel, 2015.
30. P. R. Patel, H. Zhang, M. T. Robbins, J. B. Nofar, S. P. Marshall, M. J. Kobylarek, T. D. Kozai, N. A. Kotov, and C. A. Chestek, *Journal of Neural Engineering*, **13**, 066002 (2016).
31. H. Vara and J. E. Collazos-Castro, *ACS Applied Materials & Interfaces*, **7**, 27016 (2015).
32. B. D. Bath, D. J. Michael, B. J. Trafton, J. D. Joseph, P. L. Runnels, and R. M. Wightman, *Analytical Chemistry*, **72**, 5994 (2000).
33. M. Ates, J. Castillo, A. S. Sarac, and W. Schuhmann, *Microchimica Acta*, **160**, 247 (2008).
34. B. J. Venton, K. P. Troyer, and R. M. Wightman, *Analytical Chemistry*, **74**, 539 (2002).
35. M. L. Huffman and B. J. Venton, *Analyst*, **134**, 18 (2009).
36. T. H. Yoon, E. J. Hwang, D. Y. Shin, S. I. Park, S. J. Oh, S. C. Jung, H. C. Shin, and S. J. Kim, *IEEE Transactions on Biomedical Engineering*, **47**, 1082 (2000).
37. I.-J. Cho, H. W. Baac, and E. Yoon, In *Micro Electro Mechanical Systems (MEMS), 2010 IEEE 23rd International Conference on*; IEEE, 2010, pp 995.
38. C.-H. Chen, D.-J. Yao, S.-H. Tseng, S.-W. Lu, C.-C. Chiao, and S.-R. Yeh, *Biosensors and Bioelectronics*, **24**, 1911 (2009).
39. F. Wu, E. Stark, M. Im, I.-J. Cho, E.-S. Yoon, G. Buzsáki, K. D. Wise, and E. Yoon, *Journal of Neural Engineering*, **10**, 056012 (2013).

40. B. Fan, Y. Zhu, R. Rechenberg, C. A. Rusinek, M. F. Becker, and W. Li, *Lab on a Chip*, **17**, 3159 (2017).
41. C. A. Rusinek, M. F. Becker, R. Rechenberg, and T. Schuelke, *Electrochemistry Communications*, **73**, 10 (2016).
42. G. M. Swain and R. Ramesham, *Analytical Chemistry*, **65**, 345 (1993).
43. K. B. Holt, A. J. Bard, Y. Show, and G. M. Swain, *The Journal of Physical Chemistry B*, **108**, 15117 (2004).
44. J. Cvac˘ka, V. Quaiserova, J. Park, Y. Show, A. Muck, and G. M. Swain, *Analytical Chemistry*, **75**, 2678 (2003).
45. M. Ensch, V. Y. Maldonado, G. M. Swain, R. Rechenberg, M. F. Becker, T. Schuelke, and C. A. Rusinek, *Analytical Chemistry*, **90** (11), 6477 (2018).
46. C. Dincer, R. Ktaich, E. Laubender, J. J. Hees, J. Kieninger, C. E. Nebel, J. Heinze, and G. A. Urban, *Electrochimica Acta*, **185**, 101 (2015).
47. C. E. Nebel, B. Rezek, D. Shin, H. Uetsuka, and N. Yang, *Journal of Physics D: Applied Physics*, **40**, 6443 (2007).
48. S. A. Hara, T. R. Moen, K. Bennet, K. H. Lee, and J. R. Tomshine, In *Medical Measurements and Applications (MeMeA), 2017 IEEE International Symposium on*; IEEE, 2017, pp 117.
49. D. Tryk, H. Tachibana, H. Inoue, and A. Fujishima, *Diamond and Related Materials*, **16**, 881 (2007).
50. B. Sarada, T. N. Rao, D. Tryk, and A. Fujishima, *Analytical Chemistry*, **72**, 1632 (2000).
51. Y. Qi, H. Long, L. Ma, Q. Wei, S. Li, Z. Yu, J. Hu, P. Liu, Y. Wang, and L. Meng, *Applied Surface Science*, **390**, 882 (2016).
52. P. Takmakov, C. J. McKinney, R. M. Carelli, and R. M. Wightman, *Review of Scientific Instruments*, **82**, 074302 (2011).
53. E. S. Bucher, K. Brooks, M. D. Verber, R. B. Keithley, C. Owesson-White, S. Carroll, P. Takmakov, C. J. McKinney, and R. M. Wightman, *Analytical Chemistry*, **85**, 10344 (2013).
54. R. Ramamurti, M. Becker, T. Schuelke, T. Grotjohn, D. Reinhard, G. Swain, and J. Asmussen, *Diamond and Related Materials*, **17**, 481 (2008).
55. E. Bustarret, E. Gheeraert, and K. Watanabe, *Physica Status Solidi (a.*, **199**, 9 (2003).
56. H. Xiang, Z. Li, J. Yang, J. Hou, and Q. Zhu, *Physical Review B*, **70**, 212504 (2004).
57. T. Teraji, H. Wada, M. Yamamoto, K. Arima, and T. Ito, *Diamond and Related Materials*, **15**, 602 (2006).
58. D. Narducci, C. R. Guarnieri, and J. J. Cuomo, *Journal of The Electrochemical Society*, **138**, 2446 (1991).
59. J. W. Ager III, W. Walukiewicz, M. McCluskey, M. A. Plano, and M. I. Landstrass, *Applied Physics Letters*, **66**, 616 (1995).
60. E. Gheeraert, P. Gonon, A. Deneuville, L. Abello, and G. Lucazeau, *Diamond and Related Materials*, **2**, 742 (1993).
61. M. Bernard, A. Deneuville, and P. Muret, *Diamond and Related Materials*, **13**, 282 (2004).
62. P. Kissinger and W. R. Heineman, *Laboratory Techniques in Electroanalytical Chemistry, Revised and Expanded*, CRC press, 1996.
63. J. Wang, *Analytical Electrochemistry*, John Wiley & Sons, 2006.
64. A. J. Bard, L. R. Faulkner, J. Leddy, and C. G. Zoski, *Electrochemical Methods: Fundamentals and Applications*, wiley New York, 1980; Vol. 2.
65. H. A. Strobel, W. R. Heineman, and D. T. Burns, Elsevier, 1991.